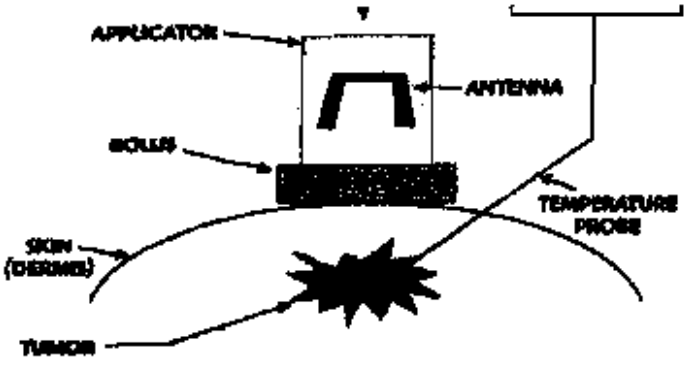

Figure 1 Schematic of the power delivery system.

In *Figure 1*, a schematic overview of the RF power delivery system is presented. A Lucite cylinder with a single ring of eight dipole antennas connected in parallel pairs sits directly over a soft tissue sarcoma of the lower leg, as shown in *Figure 3*. During treatment of Cases I and II, the applicator was positioned below the patient's knee. Filters and matching feed network were designed to deliver up to 50 W per dipole pair at a frequency of 140 MHz. Frequency selection is a trade-off between beam size and penetration depth. Higher frequencies have smaller beam widths and shorter penetration depths. A water bolus was used to reduce concomitant hot spots and to improve the radiation efficiency of the electrically short dipoles. Water is an ideal waveguide medium for two reasons. First, its electrical properties are closely matched to that of human dermis so the applied energy can be transmitted through to the tumor. Impedance mismatches and changes of wavelength at dielectric interfaces cause reflections and hot spots. Second, water has a high heat capacity and is therefore an excellent thermal coolant of the skin surface.

Figure 2 Applicator in situ.

Measuring Temperature to Confirm Simulation Results

Information about each structure and target volume of a patient can be obtained by utilizing computed tomography (CT) or other medical imaging modalities, as shown in *Figure 3*. The sarcoma tumor, located in the patient's lower leg, is surrounded by a water bolus inside a 26 cm diameter, four-antenna phased-array applicator. The patient is supine. The tumor region is indicated by white arrows. In this study, two interstitial temperature probes were inserted into the tumor and surrounding healthy tissue. These local probes were used to confirm the simulation results.

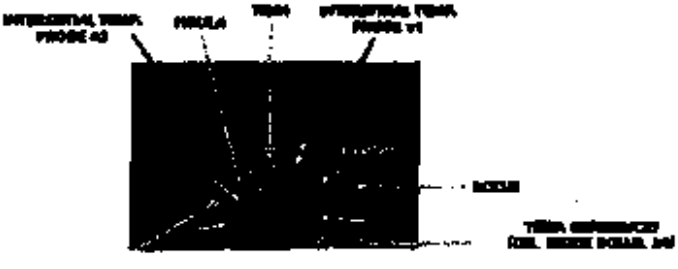

Figure 3 Cross-sectional view of sarcoma tumor.

Simulation Methods and Procedures

Due to the recent advent of accurate 3D electromagnetic and thermal simulation software programs, pre-treatment planning of complex heterogeneous tissue regions is now possible. First, the antenna array and tissue properties are entered into the EM solver with appropriate geometry, and specific absorption rate (SAR) distributions are calculated. These SAR distributions can then be automatically fed into a bio-heat transfer equation-based thermal solver to produce expected 3D temperature distributions in the tissue.

The simulation strategy is:

Step 1: Use 3D FEM simulator (HFSS) to solve for EM fields in the volume of interest.

Step 2: Insert the EM field inputs from HFSS into the 3D FEM thermodynamic simulator (ePhysics) to produce temperature distribution from bio-heat transfer equation calculations in the volume of interest with assumed perfusion values that bracket the expected range in tumor and normal tissues.

Although exact temperature maps are not possible, due to uncertain tissue perfusion which varies spatially and temporally during treatment, these SAR and estimated temperature maps help clinicians pre-plan dosage and avoid patient hot-spots. They allow technicians to determine appropriate field amplitude and phasing, which are used to control beam steering. Simulations also help engineers test new applicator designs and provide educational training aids for pretreatment planning optimization of optimal heating configurations and approaches.

In this study, an electromagnetic and thermodynamic co-simulation approach using accurate tissue properties and anatomy from a complete human body model was correlated against direct measurements. The effective energy exchange between the power delivery system and the tumor is determined in two steps. First, a 3D, finite element electromagnetic simulator is used to predict the electric field in the tissue region of interest (that is the leg). The solved electric field data are converted to SAR inputs according to the following equation:

$$SAR = \frac{1}{2} \cdot \frac{\sigma}{\rho} \cdot |E|^2 \quad \left(\frac{W}{kg}\right) \qquad (1)$$

where σ is the tissue electrical conductivity, ρ is the tissue density and E is the electric field. In the second step, the SAR data from the electromagnetic simulator is then "linked" to a thermodynamic simulator and the bio-heat transfer equation is solved for changes in temperature (ΔT):

$$\rho \cdot c \cdot \frac{\partial T}{\partial t} = \kappa \cdot \nabla^2 T - \rho \cdot \rho_b \cdot c_b \cdot F \cdot (T - T_b) + \rho \cdot SAR \qquad (2)$$

where T is the temperature (°C), t is the time (s), ρ is the tissue density (kg/m3), K is the thermal conductivity (W/(m • K)), c is the tissue specific heat (J/(kg • K)), F is the blood flow rate or perfusion (m^3/(kg • s)) and the subscript "b" refers to blood. This energy balance (Equation 2) relates the rise in temperature over time at a given region of interest to the heat inputs (power deposition or SAR) and heat losses from thermal conduction and convection (blood perfusion). As will be shown in the test case results below, the blood perfusion factor represents the greatest source of uncertainty. Several initial simulations were run to bracket the expected range of tumor perfusion. *Figure 4* summarizes the overall simulation strategy.

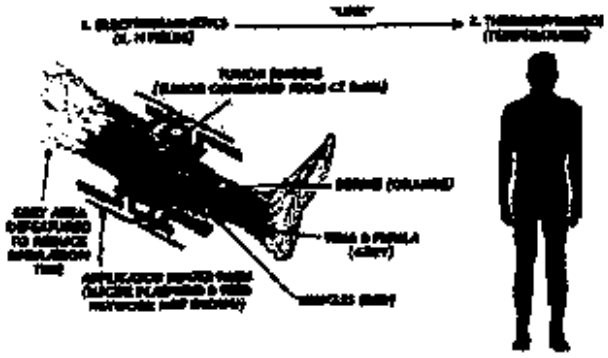

Figure 4 Summary of simulation strategy.

Procedures

Step 1: Producing the EM Model and Simulation

The applicator with paired dipole antennas and tuning stub feed network was first drawn in a mechanical CAD program. The drawing file was translated and imported into the electromagnetic simulator. The amplitude and phase inputs to each dipole were adjusted for optimum tumor focus. Next, a recently released 100-component human body model was called by the EM simulator. To reduce simulation time, all non-essential distal body components such as head or arms were de-featured (turned off).

A model of the sarcoma bearing leg was created starting from a "generic patient" computed tomography (CT) database into which the tumor volume was inserted at the appropriate location. The electrical properties were entered for each component of the model and the EM simulation initiated. The FEM-based EM simulator first produces a tetrahedral mesh for each model component using an adaptive meshing algorithm. This algorithm automatically adds more tetrahedra to regions experiencing large changes in the electric and magnetic field quantities being solved. Once the mesh is complete, the field solver solves Maxwell's equations for each tetrahedron.

The solved 3D EM field model is then linked ("data-linked") to the 1D thermodynamic solver. Data linking allows changes in the EM model, for example amplitudes and phases fed to the dipole pairs, to be automatically updated in the 3D FEM thermodynamic model. The resulting field quantities are then used to produce the SAR inputs in the thermodynamic simulator.

Step 2: Simulation of the Thermodynamic Model

APPENDIX A

MATERIAL PROPERTIES USED IN THE THERMODYNAMIC SIMULATION

	Mass Density (kg/m³)	Thermal Conductivity (W/m-°K)	Specific Heat (J/kg-°K)	Perfusion (kg/m³-s)
Muscle	1047	0.45	3550	0.44
Bone	1900	0.29	920	0.4
Marrow	1040	0.45	3550	0.44 (not found, assumed same as muscle)
Skin	1125	0.31	3000	0.39
Tumor	1047	0.53	3550	0.3 (not found, assumed a little less than other organs)

Fat (high water content but includes some fat)	1080	0.4	3300	Assumed same as muscle

Appendix A Material Properties Used in the Thermodynamic Simulation

The thermodynamic simulator uses the same 3D applicator-body model as the EM simulator. A mesh is produced and the temperature changes within each tetrahedron are derived as a function of time. To complete the thermodynamic model, material properties, including mass density, thermal conductivity and specific heat, for each component were entered. These data were derived from a literature search and are summarized in *Appendix A*.[8,9] When a range of values appeared in the literature, an average value derived from the range was used. In addition, the bolus was assumed to form a constant temperature thermal sink. Based on bolus dimensions and the volumetric flow rate of water within the bolus, an interface (forced convection boundary) temperature of 24°C was assumed.

Baseline blood perfusion values were derived from a literature search and are summarized in the table.[10] To provide a more realistic model of variable tissue perfusion during heat treatments, a temperature dependent perfusion model was created. This model was based on perfusion data of a dog's prostate taken from the *CRC Handbook of Thermal Engineering*. According to the model, the perfusion factor F, in Equation 2, was multiplied by a temperature dependent factor ranging from 1 to 1.52. This temperature dependent perfusion model was used to account for the clinical observation that perfusion increases in response to gentle heating. In addition, the perfusion value for the skin layer was assumed to increase by a factor of five when the skin is warmed. However, due to the overall mass of the skin, this additional perfusion had little effect on the simulation results.

Results

Case 1

The first case was used as a baseline to determine the correlation between measurement and simulation. As shown previously, two in situ probes were used. The first was located centrally within the tumor and the second was placed in healthy tissue to the left of the tibia. During the first 18 minutes of treatment, the four dipole pairs were driven with equal amplitudes and phases at 140 MHz.

This phasing resulted in a beam that was focused centrally in the roughly cylindrical volume of interest and heated the surrounding tissue almost equally,[3] except as modified by heterogeneous electrical and thermal tissue properties. Both the healthy tissue and malignant tissue were heated.

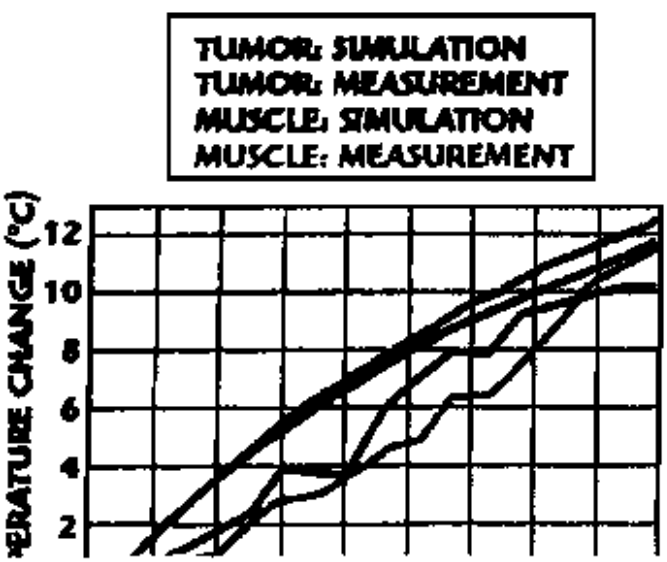

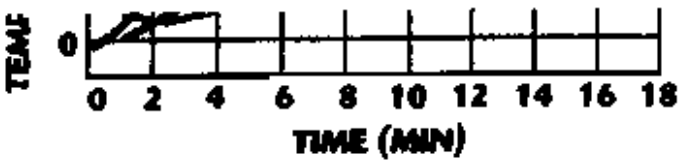

Figure 6 Case I: Temperature changes in tumor and muscle.

The temperature data for the in situ probes is compared to the simulation results in *Figure 5*. Here, the perfusion values shown in the table and the temperature dependent model were used in the simulation. A high correlation between simulation and measurement was found for both the tumor and the healthy tissue. These results were encouraging and the investigators were able to proceed to a subsequent, more complex clinical trial.

Case II

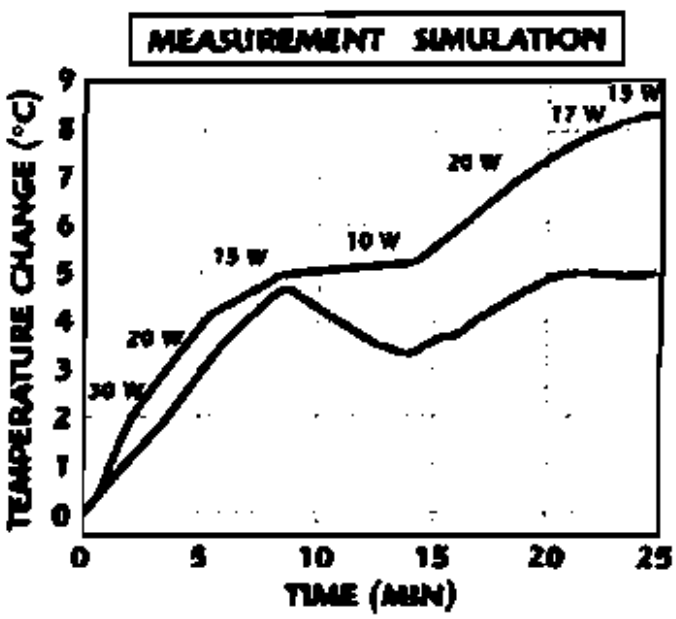

Figure 6 Case II: 25 minutes with variable power, equal phases.

In the second clinical study, an attempt was made to maintain a constant temperature rise in the tumor by adjusting the total input power to the dipole pairs during the treatment. As before, the four dipole pairs were driven with equal power and phase. For the first two minutes, 30 W were applied to each of the four dipole pairs. From minutes two to five, 20 W were applied, and so on as indicated in *Figure 6*. After the treatment, the applied power changes were simulated. As shown, there is fairly tight correlation between measurement and simulation for the first 10 minutes. Thereafter, for approximately five minutes, the curves begin to diverge. Eventually, at approximately 15 minutes, trends realign, but with a two degree separation.

After studying the data and their sensitivity to various parameters, it was postulated that the effect of perfusion was still being underestimated—even with the temperature dependent model. Subsequent simulation studies were performed to confirm this view.

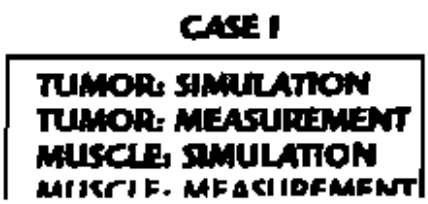

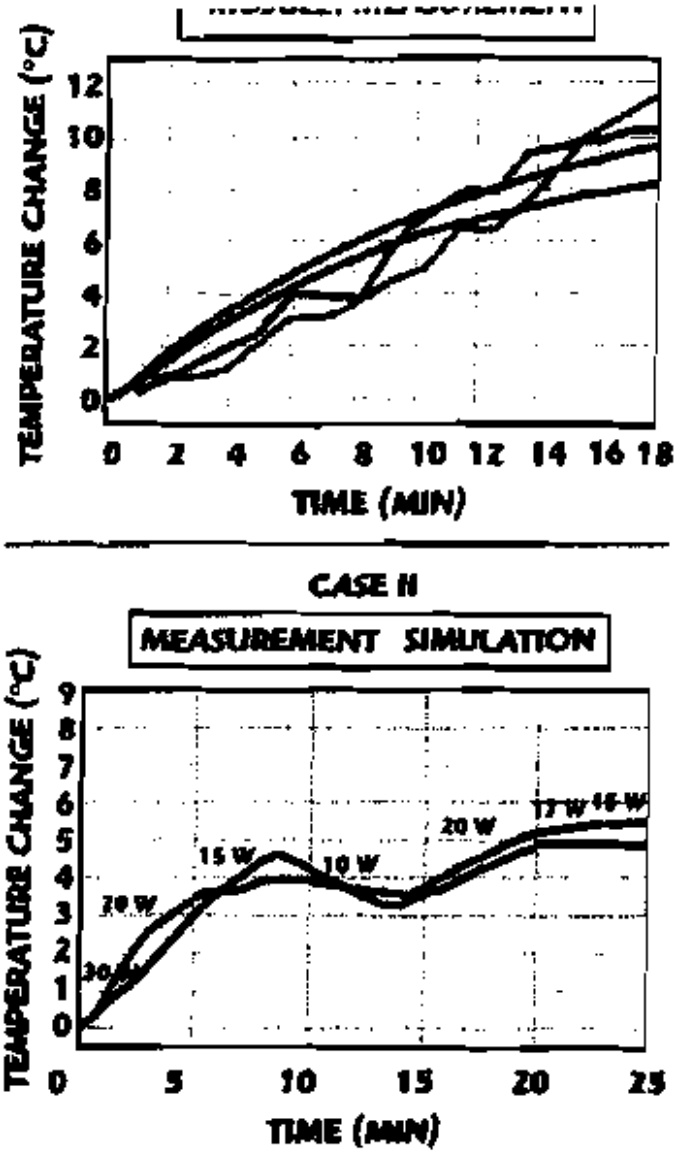

Figure 7 The effect of perfusion.

Since the sensitivity study strongly hinted that the perfusion values were too low, and since there was not enough information to include detailed modeling of complex arteries and veins during this trial, an iterative series of simulations was conducted with increasing perfusion factors. A marked improvement in the correlation in Case II was observed using a perfusion value that was double the initial value. Both cases were re-simulated with the new perfusion factors and compared to the measured results. As shown in *Figure 7*, both cases demonstrated a marked improvement in the correlation of simulated and measured data.

Discussion

A number of investigative pathways are renewing interest in adjuvant mild hyperthermia in the fight against cancer. Critical among these is the development of simulation tools that allow clinicians the opportunity to optimize the heat dosage and prevent patient hot spots. Inspired by the goal that one day researchers will be able to accurately predict the temperature distribution before a clinical hyperthermia treatment for each patient, much effort has been done in the area of computer modeling and simulation.[1] As argued in *THE LANCET Oncology* (August, 2002), "The

potential to control power distributions in vivo has been significantly improved... by the development of planning systems and other modeling tools." These simulation tools are also being used to design new applicators and train the next generation of medical researchers.

To achieve these goals, two steps are required. The first step is to determine the E-field distribution in heterogeneous tissue, which, when coupled with respective tissue properties, determines the power deposited per unit volume or mass (SAR). Secondly, using the knowledge of spatial and time dependent SAR distribution, coupled with the thermal properties, one can predict the transient and steady state temperature distributions. Ideally, one needs accurate patient specific anatomic and physiologic tissue models and complete understanding of the electrical and thermal properties of malignant and surrounding healthy tissue. Clearly, a very complex model is required. However, some of the critical information is not completely known, such as blood perfusion. Studies on blood perfusion in tumors show that the value varies significantly with tissue type, as well as temperature and other physiologic conditions.[11] But no specific value for human tumor can be identified accurately in advance. Of all these factors, the effect of local tissue temperature on muscle perfusion is the easiest to study. Research in this area has been done by different groups. The information used herein for the temperature dependence of blood perfusion is from the *CRC Handbook of Thermal Engineering*. This reference provides a few perfusion multipliers for dogs' prostate over a range of temperatures. In this study, the initial perfusion increased 17 percent when temperature exceeded 39.6°C and 52 percent when temperature reached 41.7°C.

Conclusion

In this study, a novel coupled electromagnetic and thermal simulation procedure is described that combines 3D FEM electromagnetic and thermodynamic simulators with an advanced human body model that incorporates accurate anatomic geometry and corresponding tissue properties. An assumption of temperature dependent blood perfusion has been investigated. Two clinical hyperthermia treatments of an advanced soft tissue sarcoma of the leg are simulated and results compared to simulations. The comparison of simulated and measured thermal data are shown to have a high degree of correlation if blood perfusion is considered, proving the importance of perfusion modeling for clinical applications.

Acknowledgments

This project was supported by NIH grant 1P01-CA042745. The authors would like to express their appreciation to a large number of collaborators at Duke University Medical Center who participated in collaborative efforts that contributed to the investigation reported here. The first author also gratefully acknowledges the support and helpful discussions from the software development group at Ansoft Corp.

References

1. S.B. Field and J.W. Hand, *An Introduction to the Practical Aspects of Clinical Hyperthermia*, Bigger Books, 1990.

2. J. v.d. Zee, "Heating the Patient: A Promising Approach," *Annals of Oncology*, Vol. 13, No. 8, August 2002, pp. 1173-1184.

3. M.W. Dewhirst, L. Prosnitz, D. Thrall, D. Prescott, S. Clegg, C. Charles, J. MacFall, G. Rosner, T. Samulski, E. Gilette and S. LaRue, "Hyperthermic Treatment of Malignant Diseases: Current Status and a View Toward the Future," *Seminars on Oncology*, Vol. 24, 1997, pp. 616-625.

4. A.J. Fenn and G.A. King, "Adaptive Radiofrequency Hyperthermia Phased-array System for Improved Cancer Therapy: Phantom Target Measurements," *International Journal of Hyperthermia*, Vol. 10, 1994, pp. 189-208.

5. Y. Zhang, W.T. Joines, R.L. Jirtle and T.V. Samulski, "Theoretical and Measured Electric Field Distributions Within an Annular Phased Array: Consideration of Source Antennas," *IEEE Transactions on Biomedical Engineering*, Vol. 40, No. 8, August 1993, pp. 780-787.

6. P. Wust, R. Beck, J. Berger, H. Fähling, M. Seebass, W. Wlodarczyk, W. Hoffman and J. Nadobny, "Electric Field Distributions in a Phased-array Applicator with 12 Channels: Measurements and Numerical Simulations," *Medical Physics*, Vol. 27, No. 11, November 2000, pp. 2565-2579.
7. L. Wu, R.J. McCough, O.A. Arabe and T.V. Samulski, "An RF Phased-array Applicator Designed for Hyperthermia Breast Cancer Treatments," *Physical Medical Biology*, Vol. 51, No. 1, January 2006, pp. 1-20.
8. H.S. Hatfield and L.G.C. Pugh, "Thermal Conductivity of Human Fat and Muscle," *Nature*, Vol. 168, No. 4282, November 24, 1981, pp. 918-919.
9. H.F. Bowman, "Heat Transfer and Thermal Dosimetry," *Journal of Microwave Power*, Vol. 16, No. 2, 1981, pp. 121-133.
10. L. Shargel and A.B.C. Yu, *Applied Biopharmaceutics and Pharmacokinetics*, Fourth Edition, McGraw Hill/Appleton and Lange, 1999.
11. S. Fujita, M. Tamatsuka and K. Kuroda, "Effects of Perfusion Rate on the Optimization of RF-Capacitive Hyperthermia," *IEEE Transactions on Biomedical Engineering*, Vol. 45, No. 9, September 1998, pp. 1182-1186.

Copyright © 2009 Microwave Journal & Horizon House Publications®.
All rights reserved.

Sidebar: Towards the Validation of a Commercial Hyperthermia Treatment Planning System

After submitting the article to Microwave Journal, a better reference for blood perfusion was found. Simulations were done with the temperature dependent expressions found in this reference.[1] It is known that the outer layer of the tumor has plenty of blood vessels. Therefore, the outer 30% has been given the same perfusion as muscle in the simulation. This resulted in the plot shown here.

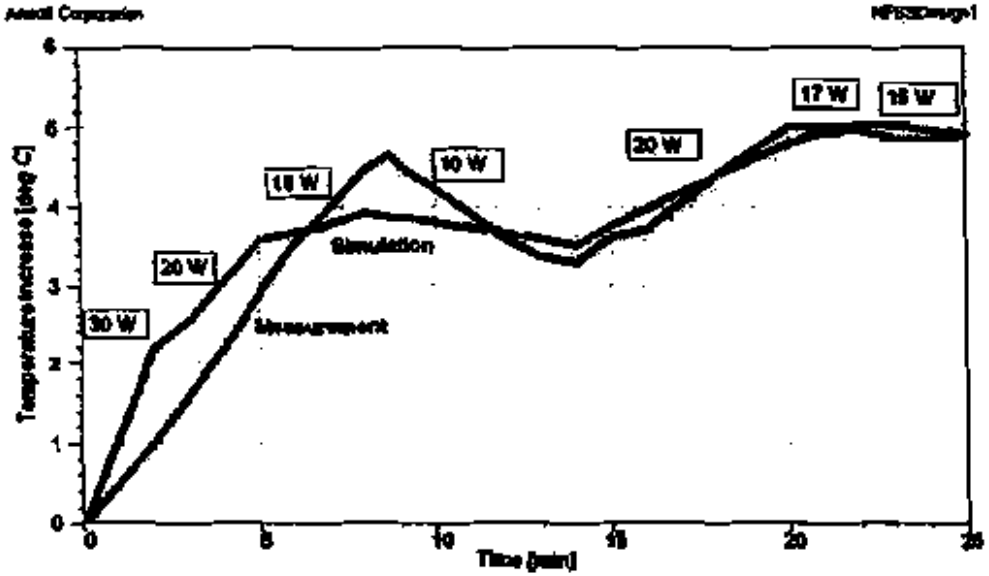

Results remain very sensitive to perfusion. For instance, if the aforementioned 30% is replaced by 20%, the final temperature increases by 0.7 deg C. Even with this sensitivity, it appears that the final temperature can be predicted within a reasonable band. This enables treatment planning with simulation.

[1] B. Erdmann, J. Lang, and M. Seebass, "Optimization of temperature distributions for regional hyperthermia based on a nonlinear heat transfer model," Ann. N. Y. Acad. Sci., vol. 858, pp. 35–46, Sep. 11, 1998.

EXHIBIT C

Sony Ericsson

Generic Phone SAR Comparison

Simulations performed by IEEE [illegible] TC34 SC2

Sony Ericsson

Phone model

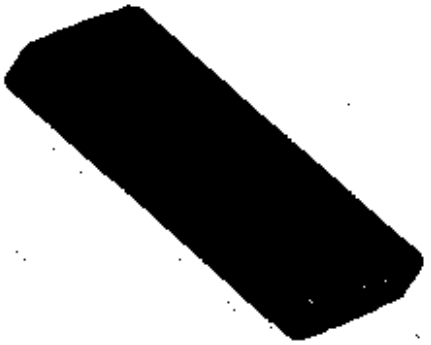

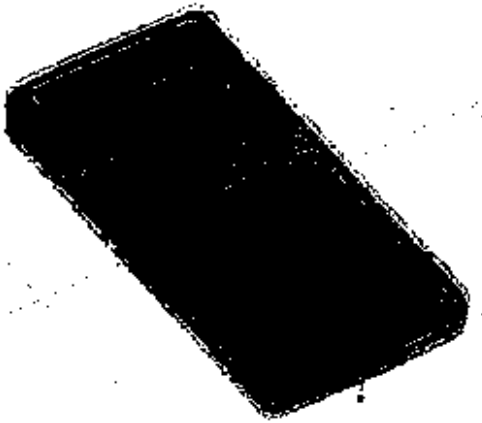

PIFA

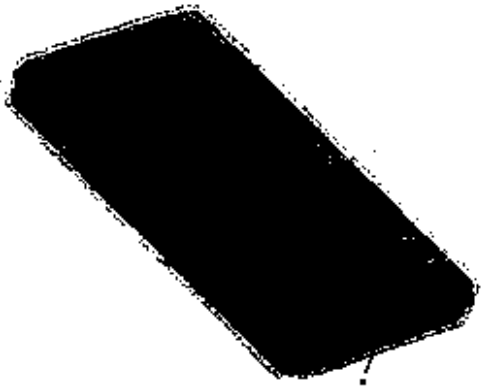

Metal parts

Phone + SAM head

General design
Size: ≈ 100 x 55 mm
Frequencies: 900/1800 MHz

Sony Ericsson

SAR @ 900 MHz for 1 W accepted power

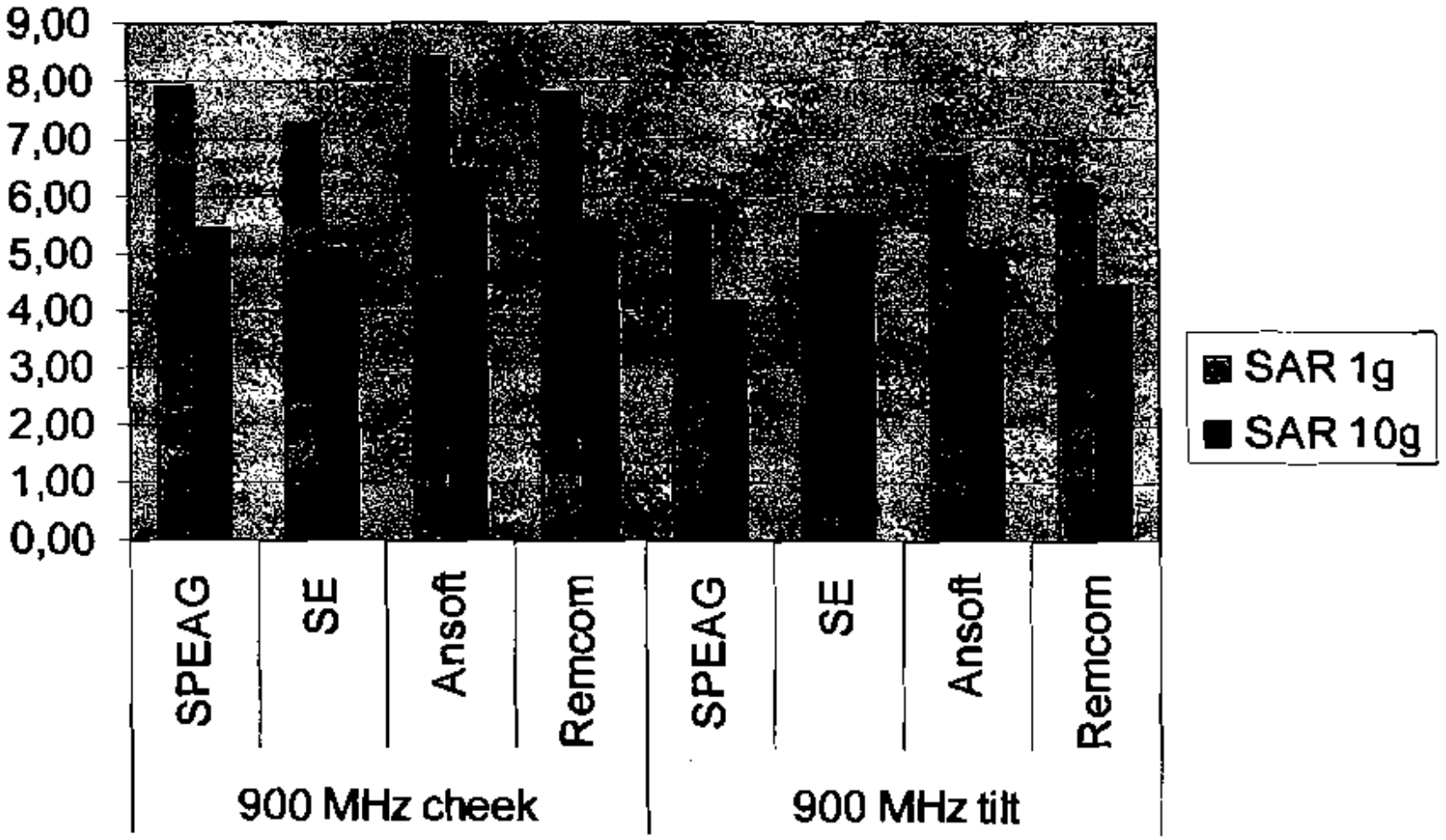

Sony Ericsson

SAR @ 1800 MHz for 1 W accepted power

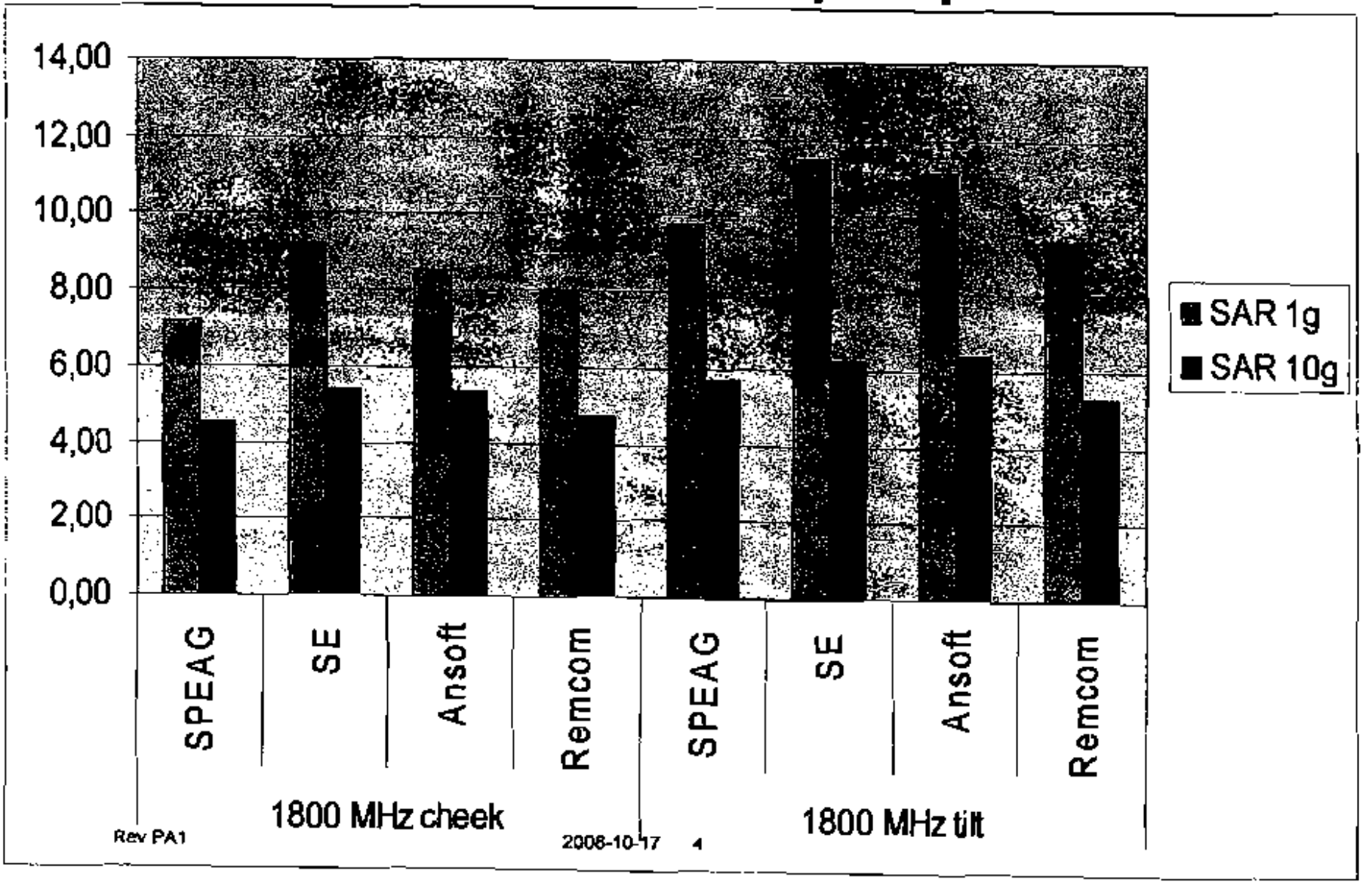

EXHIBIT D

Strategies for Effective Use of EM Simulation for SAR

Part I: Standards-compliant Simulations Using Finite Element Analysis

Matt Commens
Ansoft Corporation
Pittsburgh, PA
mcommens@ansoft.com

Lawrence Williams
Ansoft Corporation
Pittsburgh, PA
lwilliams@ansoft.com

Abstract—Specific absorption rate (SAR) is computed using the finite element method (FEM) embedded in Ansoft HFSS. Comparisons to finite difference time domain (FDTD) simulations and measurements show that accurate results can be obtained using FEM. High-fidelity models using standards-compliant phantom models are demonstrated and benefits of FEM are highlighted.

Keywords-specific absorption rate, SAR, design automation, FDTD, FEM, HFSS

I. Introduction

The use of mobile and portable wireless devices continues to experience rapid growth worldwide. Interaction of electromagnetic fields with the human body remains a prevalent topic especially due to the health concerns over increasing cellular telephone usage. Standards organizations have set exposure limits in terms of the specific absorption rate (SAR) that takes into account the field intensity in relation to the material density. Electromagnetic field simulation has proved to be a useful tool for predicting the field exposure due to particular telephone handset configurations. The vast majority of these simulations have been performed using tools based on the finite difference time-domain (FDTD) method. In this paper, it will be shown by example that simulations based on the finite element method (FEM) can be used to provide highly-accurate simulation of SAR on complex models. Examples that include a spherical phantom for validation and a standards-compliant phantom model for the human head will be considered. Benefits of the finite element method for computing high-fidelity field and specific absorption rate plots will be highlighted.

II. Specific Absorption Rate

SAR is defined as the time rate of energy absorbed in an incremental mass, divided by that mass. Average SAR in a body is the time rate of the total energy absorbed divided by the total mass of the body. Typically SAR is reported in watts per kilogram and it is assumed that the value is calculated over 1g/cm3 of tissue.

III. Phantom Model

Phantoms are used for wireless device compliance testing to hold a liquid mixture that is representative of human tissue. The phantom and fluid mixtures are important factors for determining SAR since the size and tissue properties affect how much incident energy is absorbed. The use of a common phantom among researchers and designers increases the probability of producing repeatable measurements by providing guidelines for positioning and testing the wireless device. An example of a common phantom model is shown in Figure 1.

Figure 1. Example human phantom model.

IV. Applications of HFSS For SAR

Ansoft HFSS is an ideal tool for simulating wireless devices and calculating SAR. The finite element method utilized by HFSS provides a robust conformal mesh generator that can solve Maxwell's equations for complex, arbitrarily-shaped objects with devices and structures in arbitrary orientations. The method allows direct representation of lossy dielectrics in the frequency domain. Excitation ports can be placed anywhere within the model allowing users to stimulate the electric and magnetic fields at any user-defined location.

A. Spherical Phantom Validation

To demonstrate the effectivness of HFSS for simulating SAR, a model of a spherical phantom will be simulated and compared to measurements and to simulations based on FDTD. Figure 2 depicts the spherical phantom to be used for the comparisons. The spherical phantom is a glass bowl with an opening at it northern hemisphere. The opening allows a measurement probe to move within the liquid. It has been determined that the opening does not alter the fields in the southern hemisphere. Dimensions of the sphere are as follows:

Inner radius = 106.5+/-5mm
Thickness = 5+/-0.5mm.
Opening = d2 =170mm
$\varepsilon_r = 4.6$.

The antenna used for measurements is a symmetrical dipole constructed according to the IEEE SCC 34, WG1, "Spherical Phantom Experimental Protocol, Draft F".

Overall Length = 168mm
Gap between dipoles = 1mm
Wire Diameter = 3.6mm.

The following liquid dielectric properties were measured:

ε_r = 43.32 +/-5%
σ = 0.862 +/-10%
ρ = 1.33 kg/m3 (For the SAR evaluations, the density will be assumed to be 1 kg/m3).
Level = d1 = 13.4 cm.

Computations were performed at 11 different positions of the dipole antenna as depicted in Table 1. Ansoft Optimetrics was used to automate the simulations. With the dipole placed at the center of the bowl, the antenna feed point impedance is calculated at varying distances from the bowl (b=5mm, 25mm, 50mm). In addition, the dipole is positioned such that the tip (Left and Right) of the dipole is located at the center of the spherical phantom. The distance between the dipole and the phantom is measured from the top of the dipole to the outer south pole of the bowl.

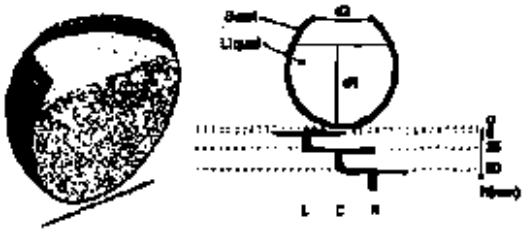

Figure 2. Spherical phantom to be used to compare with FDTD and measurements.

In some forums there has been intuition that the asymmetric mesh produced by HFSS might adversely affect the results of the simulations. These comments have primarily been made due the familiarity of FDTD for SAR analysis and it's symmetric brick mesh. Performing simulations with the dipole located at the left and right tip of the bowl should yield the same answer due to the symmetry of the model (independent of the mesh). Performing both simulations revealed that no discernible asymmetrics were produced in the result. This solution symmetry between the right and left positions (for HFSS) demonstrates that the non-uniform mesh generated by the adaptive meshing does not adversely affect the simulation results. By using a non-uniform mesh that conforms to the model, Ansoft HFSS concentrates the mesh in the area of interest thereby improving the efficiency of the solver.

Table 2 provides a comparison between measured, FDTD, and HFSS simulations for the spherical phantom. Nokia provided the measurements and FDTD results. As can be seen in the Table, HFSS consistently provides results that are in close agreement with the measured data.

Table 1. Dipole locations used for the simulations.

b	L	C	R
0	1	0	1
5	1	1	1
25	1	1	1
50	1	1	1

Table 2. Comparison between measured, FDTD, and HFSS for spherical phantom.

Position	b (mm)	Meas., Re(Z) [Ω]	Meas., Im(Z) [Ω]	FDTD, Re(Z) [Ω]	FDTD, Im(Z) [Ω]	HFSS, Re(Z) [Ω]	HFSS, Im(Z) [Ω]
Center	5	48.3	-8.3	77.3	-4.44	46.5	-2.43
Center	25	51.6	25.4	79.3	23.3	50.0	14.12
Center	50	70.2	23.2	86.3	42.8	66.5	20.6
Right	0	102.4	95.8	243.7	128.8	111.9	70.5
Right	5	81.5	44.6	134.7	35.1	87.9	31.7
Right	25	74.0	24.1	111.3	25.7	75.7	16.4
Right	50	83.4	18.1	104.8	37.1	78.7	14.1
Left	0	103.7	92.4	222.2	123.8		
Left	5	80.5	43.8	124.7	35.4		
Left	25	74.1	23.9	111.6	26.0		
Left	50	82.6	18.9	105.2	37.5		

8. *SAM (Specific Anthropomorphic Mannequin) Phantom*

A more comprehensive analysis is obtained when using a more realistic human head phantom. The IEEE has created a standard human head phantom for use when simulating SAR in the presence of radiating structures see IEEE SCC34 P1528-2002 (Draft CD 1.1 - Dec. 29, 2002). Figure 3 contains images of the SAM phantom as modeled in HFSS. Material properties in the 1800-2000 MHz range are modeled using $\varepsilon_r = 40.0$ and $\sigma = 1.78$ S/m.

Figure 3. Human head SAM phantom IEEE SCC34 P1528-2003 as modeled in HFSS.

Simulations of the SAM model were performed using an accurate representation of a cellular telephone handset. The handset is a "flip-phone" design with a helix-loaded monopole antenna. Figure 4 is an image of the HFSS model depicting the orientation of the handset. The handset model includes the antenna, LCD, PCB ground, and several other large perfect electric conductor components. These items were modeled by assigning appropriate boundary conditions and material properties. Figure 5 is a close-up view of the handset antenna and its coax feed port. Figure 7 is a plot of the average SAR on a line traversing from the handset to the center of the SAM phantom.

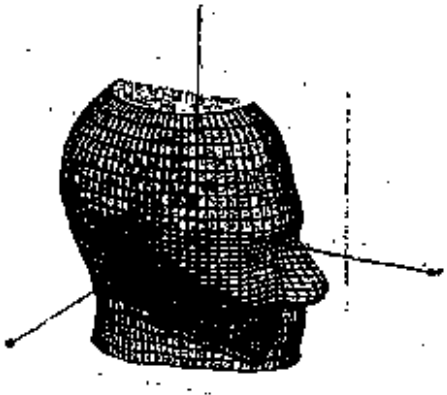

Figure 4. HFSS model depicting handset orientation.

Figure 5. Close-up view of the handset antenna and coax feed port.

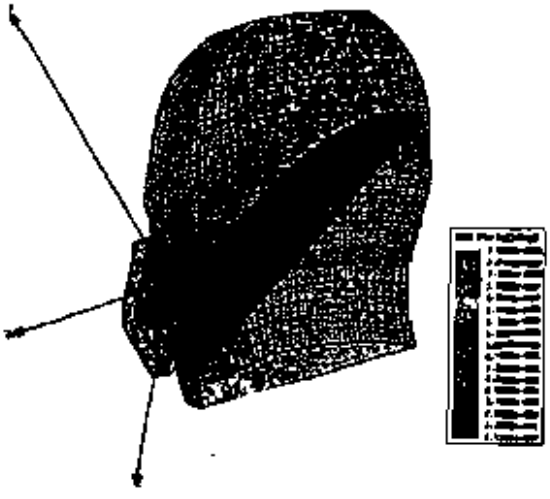

Figure 6. SAR plot as computed by HFSS at 1.8 GHz

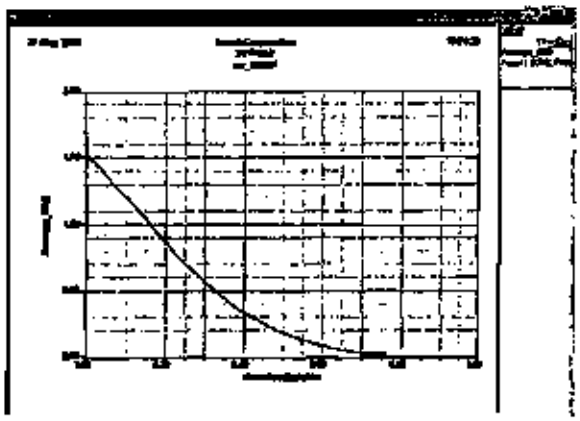

Figure 7. Average SAR as a function of position.

V. Conclusion

Interaction of electromagnetic fields with the human body remains a prevalent topic especially due to the health concerns over increasing cellular telephone usage. Electromagnetic field simulation has proved to be a useful tool for predicting SAR, and the vast majority of these simulations have been performed using tools based on the finite difference time-domain (FDTD) method. In this paper, it was shown that the finite element method can be used to compute high-fidelity maps of SAR. A validation case using a spherical phantom validated the FEM accuracy and simulation using standards-compliant phantom model demonstrated the capacity to solve high-resolution cases. Benefits of the finite element method for computing high-fidelity field and specific absorption rate plots were highlighted.

Acknowledgement

Special thanks to Nokia for providing the FDTD and measured results for the spherical phantom. Gratitude is extended to Steve Rousselle and Charly Jenny of Ansoft Corporation for the simulations.

EXHIBIT E

Ansoft HFSS Analysis of Specific Absorption Rate for Flat Phantom Measurement Standard Outlined in IEEE P1528-2002:

Recommended Standard for Determining the Spatial Peak Specific Absorption Rate (SAR) in the Human Head from Wireless Communication Devices: Measurement Technique

Matthew H. Commens, Ph.D.
Applications Engineer
Ansoft Corporation
mcommens@ansoft.com
412-261-3200

The table below summarizes the data from an Ansoft HFSS analysis of flat phantom models as described in the IEEE draft standard for SAR measurements.

HFSS results: Compared to measured data from Table 8-1 of paper

Freq. (MHz)	1g SAR Measured	1g SAR HFSS v11	10g SAR Measured	10g SAR HFSS v11	L SAR fp Measured	L SAR fp HFSS v11	L SAR 2cm Measured	L SAR 2cm HFSS v11
300	3.06	3.05	2.07	2.06	4.63	4.61	2.20	2.16
450	4.98	4.93	3.31	3.30	7.59	7.57	3.28	3.26
835	9.62	9.56	6.26	6.23	14.71	14.82	4.93	4.89
900	10.98	10.95	7.02	7.00	17.01	17.15	5.47	5.46
1450	29.83	29.77	16.50	16.48	53.90	54.23	6.54	6.35
1800	39.36	38.81	20.45	19.99	74.39	74.34	6.85	6.36
1900	40.97	40.92	21.21	21.10	78.02	77.96	6.54	6.84
2450	55.42	55.35	25.42	25.39	115.00	115.74	8.09	7.49
3000	65.81	65.78	26.48	26.42	157.66	159.21	8.8	9.43

In general there is excellent agreement between the HFSS simulations and measurements. The possible exception would be the Local SAR above the feedpoint. This is likely due to the use of 50 Ω lumped gap sources as an approximation to the balun feed for the dipoles.

Included with this report is a fully parameterized HFSS v1 project with 9 separate HFSS simulations. Two symmetry planes were exploited to reduce problem size.

Relevant data for the analysis can be found in the paper:

Material data for brain tissue: Page 39, Table 5-1
SAR results: Page 70, Table 8-1
Flat phantom and dipole measurement parameters: Page 70, Table 8-2
Dipole dimensions: Page 146, Table G.1

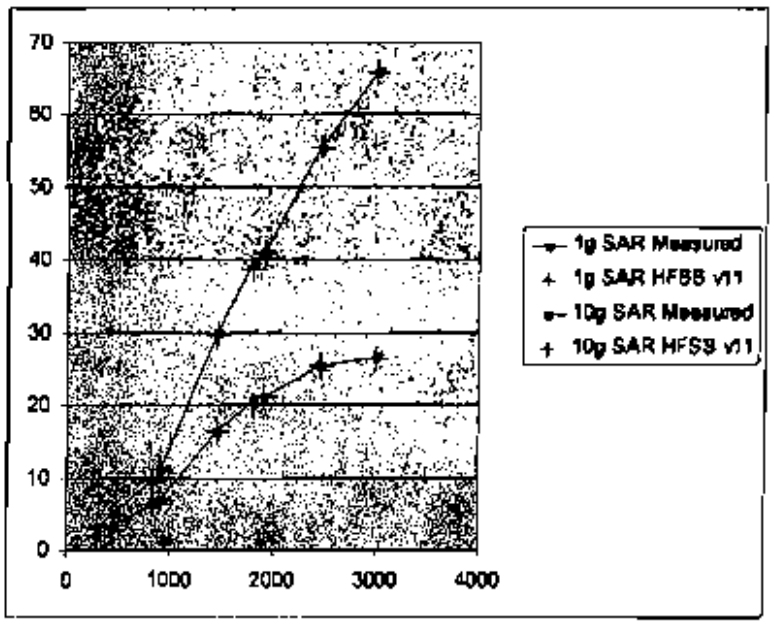
70
60
50
40
30
20
10
0
0
1000
2000
3000
4000
1g SAR Measured
1g SAR HFSS v11
10g SAR Measured
10g SAR HFSS v11

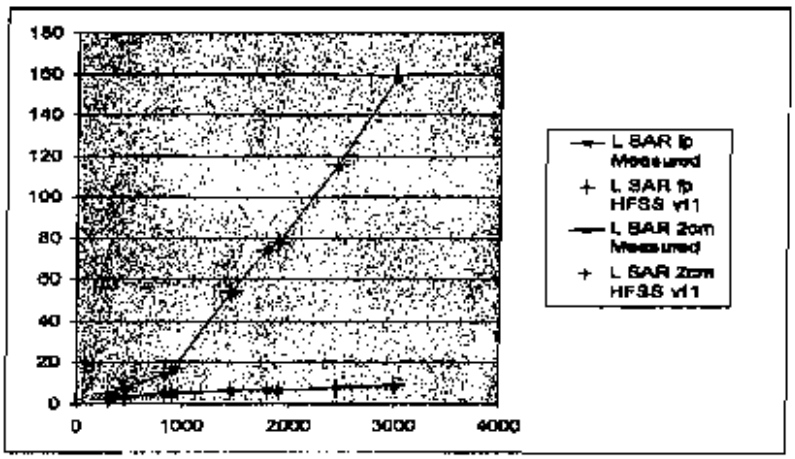
180
160
140
120
100
80
60
40
20
0
0
1000
2000
3000
4000
L SAR fp Measured
L SAR fp HFSS v11
L SAR 2cm Measured
L SAR 2cm HFSS v11

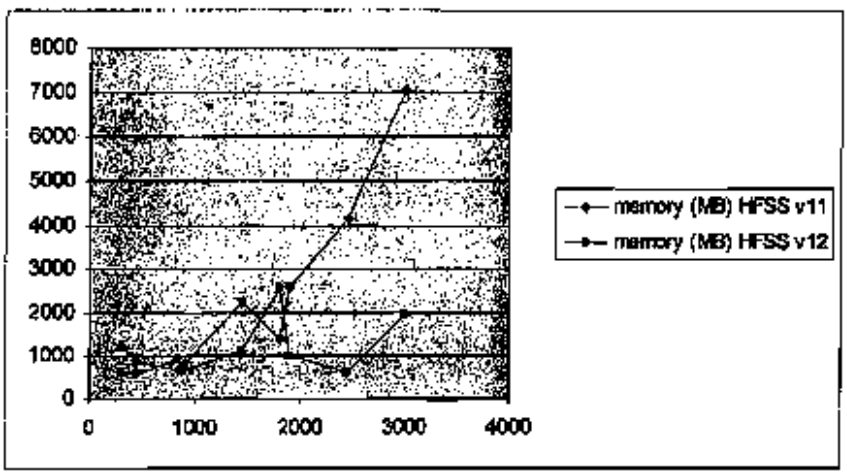
8000
7000
6000
5000
4000
3000
2000
1000
0
0
1000
2000
3000
4000
memory (MB) HFSS v11
memory (MB) HFSS v12

EXHIBIT F

SAR Assessment in a Human Head Model Exposed to Radiation from Mobile Phone Using FEM

S. Selim Şeker
Boğaziçi University, Electric-Electronic Engineering Department, Bebek, İstanbul,TR.
e-mail:seker@boun.edu.tr

B. Ozsoy Demirbilek
Boğaziçi University, Institute of Biomedical Engineering, Bebek, İstanbul,TR

Avni Morgul
Boğaziçi University, Electric-Electronic Engineering Department, Bebek, İstanbul,TR.

Abstract

It is important to be able to quantify both the absorption of electromagnetic energy in the human body and the resulting thermal effect. In this study, the specific absorption rate (SAR) of electromagnetic radiation from mobile phones on the human head was investigated.

As it is not possible to perform the experiments on human in vivo, the human head and the antenna radiated in 900 MHz were simulated. In this study, the spherical model as single layer and three layers was simulated by using Agilent High Frequency Structure Simulator, which employs the finite element method (FEM), and the EM power absorption rate of tissue was calculated by a C++ program. The results were compared with the results of the studies in the literature and a good agreement was obtained.

To evaluate the efficiency of the method, a rat head was simulated and the results were compared with the experimental results obtained from the in vivo experiments conducted on the rats.

Keywords

SAR, FEM, Modeling of human head, Mobile phone.

INTRODUCTION

The most investigated effect of EM energy on biological tissues is the transformation of energy entering the tissues into increased kinetic energy of the absorbing molecules, thereby producing a general heating in the medium. The power absorbed by the tissues will produce a temperature rise that is dependent on the cooling mechanism of the tissue. The patterns of the fields producing the heating are complex functions of the frequency, source configuration, tissue geometry and dielectric properties of the tissues. When the thermoregulatory capability of the system is exceed, tissue damage result.

When a biological system is exposed to microwave radiation, an internal field is induced in the system. To calculation of this internal field is named as dosimetry [1]. The electromagnetic energy absorbed per unit mass of tissue is called specific absorption rate (SAR) [1]:

$$SAR = E_i^2 \frac{\sigma}{2\rho} \qquad (1)$$

where; σ: conductivity (mS^2/m), ρ: density of tissue (kg/m^3), E_i: internal electrical field (V/m).

The development of models to predict the absorption of electromagnetic energy and the physiologic thermoregulatory response for the human body has proceeded for several years. Few studies are summarized here as follows:

In 1986, Arthur W. Guy et al. studied on quantification of the SAR-patterns in human models exposed to UHF mobile-antenna fields using thermography, nonperturbing temperature probes and E-field sensitive diodes [2]. The exposure conditions included man, woman, and child models in different positions. In this study, full-scale phantom models, which were filled with synthetic gel having the same dielectric properties as human muscles, were used. The result of this study was "the mobile-antenna system could be operated safely with all of the ANSI RFPG exposure guides in terms of both power density and maximum SAR".

In 2000, Nikita et al. studied interaction between a Layered Spherical Head Model and a finite-length dipole antenna by the method based on the combination of the Green's function method with the MAS (method of auxiliary sources) [3].

In 2000, Mangoud et al. combined the frequency-domain method of moments (MoM) and FDTD for the simulation of human interaction with cellular phones [4]. The results of the tests were in excellent agreement with published results and expectations. This method was useful for analyzing complex problems.

On the other hand, medical researchers have been studying thermal effects and changes on the ear. In one of these studies, W.B. Noyes and al. reported that moderate changes in cochlear temperature (3-4 degrees) of rabbits did not produce irreversible thermal damage to the cochlear outer hair cells [5]. W. Keck and al. studied conduction of thermal stimuli in the human temporal bone [6] and reported that the temperature difference across the horizontal semicircular canal was of shorter duration than the absolute temperature change.

As it can be seen, the studies on electromagnetic radiation of cellular phones on the human head were performed either by using the FDTD, FD, Moment Method or phantoms. In our study, the FEM was used and compared with the literature.

The calculation of the internal field is difficult to achieve because of many dependent factors; therefore, mathematical techniques that consist of numerically solving Maxwell's equations are generally used in the computer simulation. In numerical techniques, Maxwell's equations can be solved as

0-7803-7264-6/02/$17.00 © 2002 IEEE

a set of linear equations by matrix inversion or by iterative techniques. Generally, two numerical methods are employed:

1. The moment method
2. Finite-element or finite difference approaches

The Finite Element Method, which was used in this study, has its origin in the field of structural analysis. The application of FEM becomes easier with the problems having irregularly shaped boundaries because the use of tetrahedral elements allows curved surfaces to be approximated much more accurately than is possible by cubical blocks used in the Method of Moment and the Finite Difference Method [7].

In this study, the simulation was performed using HP Agilent High Frequency Structure Simulator. Agilent HFSS is a software package for electromagnetic modeling of passive, three-dimensional structures. It computes scattering parameter (S-parameter) response for multiple modes, electric field distributions including far-field antenna radiation patterns, impedance and propagation constants for multiple modes. The package uses Maxwell's equations to solve for electric and magnetic fields and includes dispersion; uses AutoCAD program to handle unrestricted geometries and employs the finite element method. The solution is performed at a single frequency or over a range of frequencies. The post processor of the software makes possible to view and analyze the simulation data that include E and H fields, far field, and antenna parameters.

MULTILAYERED-SPHERICAL MODEL OF HUMAN HEAD

Multilayered Spherical Model, which approximates the primate cranial structure irradiated by plane wave in the cellular frequencies range, was used to model human head by Shapiro in 1971 [8]. Weil extended his work in 1975 to study the effect of hotspot shift with changes in frequencies [9].

To solve the dosimetry problem caused by electromagnetic radiation on human body is too complicated. As a result we only model the electromagnetic effects on the human head. Figure 1 shows that the basic spherical model with a plane wave, polarized in the x-direction and propagating in the z-direction, incident upon it [9].

The model consists of a core of brain-like material (region, P=1) surrounded by six concentric layers of different materials. The seventh layer, P=7 represents the air.

The electric fields induced in a sphere or spherical layer of tissue by an incident plane wave field can be calculated from the general vector spherical wave solutions of the wave equation, which is based on Mie Theory and formulated Stratton. Mathematical details have been given by Shapiro et al [8]. The basic solution involves expanding the incident and secondary (scattered and internally induced) fields into vector spherical harmonics.

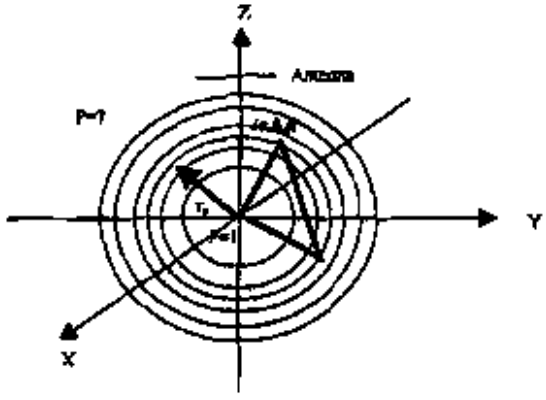

Figure 1. Plane wave incident upon spherical model with six concentric shells and the location of the dipole antenna on yz plane.

Although the modeling human head in six layers is more realistic, it is possible to model human head in single layer or in three layers [3]. In our study, a single layered and three layered spherical models with diameter of 20 cm were used to model human head and for a single-layered model, the dielectric constant ε_r of the human head was taken as 39.5 and dielectric loss tangent, which is $\varepsilon''/\varepsilon'$, as 0.354, σ as 0.9 and ρ as 1100 [3]. For three-layered modeling, the following values were used.

Table I The tissues and the properties used in simulations

Layer	Tissue Modeled	Thickness (cm)	Relative Permittivity ε_r	Conductivity σ (mho/m)	Density ρ (kg/m³)	Loss Tangent ($\varepsilon''/\varepsilon'$)
1	Brain	9.10	56.8	0.9	1050	0.387
2	Bone	0.50	12.5	0.11	1200	0.272
3	Skin	0.40	39.5	1	1100	0.354

Modeling Dipole Antenna and the Human Head

The antenna used in simulation was modeled as a dipole antenna with the length of 5 cm. The voltage source was located in the center gap of the dipole antenna. The output power was 1 W. The distance between head and antenna was 1.45 cm.

Simulation

The finite element mesh was created for the structure. The accuracy of the solution depends on how small each of the individual elements (tetrahedra) is. It was possible to refine the mesh size in the program. But, generating a field solution for meshes with a large number of elements required a significant amount of computing power and memory.